#### Contents lists available at ScienceDirect

# Petroleum Science

journal homepage: www.keaipublishing.com/en/journals/petroleum-science



# **Original Paper**

# Differential tectonic evolution and formation mechanism of three subsags in Wenchang Sag of Pearl River Mouth Basin, South China Sea



Qiu-Gen Zheng <sup>a</sup>, Jun-Liang Li <sup>b</sup>, Bao-Hua Lei <sup>c, d, \*</sup>, Peng Song <sup>b</sup>, Qi Li <sup>a</sup>, De-Feng Shi <sup>b</sup>, Hao Liu a. Chang-Song Lin a

- <sup>a</sup> School of Ocean Sciences, China University of Geosciences (Beijing), Beijing, 100083, China
- <sup>b</sup> Hainan Branch of the China National Offshore Oil Corporation, Haikou, Hainan, 570311, China
- <sup>c</sup> Qingdao Institute of Marine Geology, Qingdao, Shandong, 266237, China
- d Laboratory for Marine Mineral Resources, Pilot National Laboratory for Marine Science and Technology (Qingdao), Qingdao, Shandong, 266237, China

#### ARTICLE INFO

#### Article history: Received 29 June 2022 Received in revised form 7 November 2022 Accepted 23 November 2022 Available online 28 November 2022

Edited by Jie Hao and Teng Zhu

Keywords: Strike-slip stress Releasing bend Restraining bend Double restraining bend Structural inversion Zhu III South fault Wenchang sag Northern South China Sea

#### ABSTRACT

Notable differences in the structural characteristics and evolution of three adjacent sub-sags, i.e., the Wenchang sub-sags A, B, and C, on the downthrown side of the Zhu III South Fault in the Wenchang Sag, are significant as they affect the formation and distribution of the oil and gas in these three sub-sags. However, the differences in their tectonic evolutions and formation mechanisms have not yet been adequately explained. In this paper, stress analysis, equilibrium profiles, and paleogeomorphic restoration, are used to investigate the dynamic settings, formation mechanisms, and influencing factors of the structural deformation related to the formation of the Wenchang Sag based on interpretation of seismic data. The results of the stress analysis suggest clockwise deflection of the regional tensile stress direction from a WNW-ESE trend during the Early Paleocene to NW-SE and NNW-SSE trends during the Eocene, to a nearly N-S trend during the Oligocene, and finally to a NNE-SSW trend during the Miocene. This clockwise rotation of the regional tensile stress direction led to the formation of a dextral strike-slip stress component parallel to the NE-trending Zhu III South Fault. This strike-slip stress component formed a releasing bend in sub-sag A, and may be associated with the continuous subsidence of a thick sedimentary layer in sub-sag A. It also created a restraining bend in sub-sag B, which underwent multiple structural inversions during its extension and subsidence and has a relatively small sedimentary thickness. The double restraining bend in sub-sag C is considered to have been strongly uplifted and eroded in response to this strike-slip stress component. Four obvious structural inversions in sub-sag B are identified in this paper. These structural inversions correspond to the last four regional tectonic movements. This interpretation suggests that the formation of the structural inversions was likely related to the strong tensile stress and the small intersection angle between the direction of the regional tensile stress and the pre-existing boundary fault. The rotation of the tensile stress direction was responsible for the strike-slip movement on the pre-existing boundary fault and the formation of the releasing bend and restraining bend, which controlled the structural evolutions of the sub-sags. This reasonably explains the differential tectonic evolution of these three sub-sags in the Wenchang Sag, and provides a crucial idea for structural analysis of similar basins.

© 2023 The Authors. Publishing services by Elsevier B.V. on behalf of KeAi Communications Co. Ltd. This is an open access article under the CC BY-NC-ND license (http://creativecommons.org/licenses/by-nc-nd/

4.0/).

#### 1. Introduction

The Pearl River Mouth Basin (PRMB) is the largest oil-bearing

E-mail address: lbaohua@mail.cgs.gov.cn (B.-H. Lei).

rift basin in the northern margin of the South China Sea (SCS) (Fig. 1a), and its intricate system of fault structures plays a vital role in controlling the sedimentation and oil accumulation (Zhu et al., 2016; Bao et al., 2017; He et al., 2017; Deng et al., 2020; Mu et al., 2022). In the PRMB, several studies have been conducted on the extension orientations of the faulted basins, which shifted from NNE, NE, and NEE to nearly EW throughout the deposition of the

<sup>\*</sup> Corresponding author. Qingdao Institute of Marine Geology, Qingdao, 266237, China.

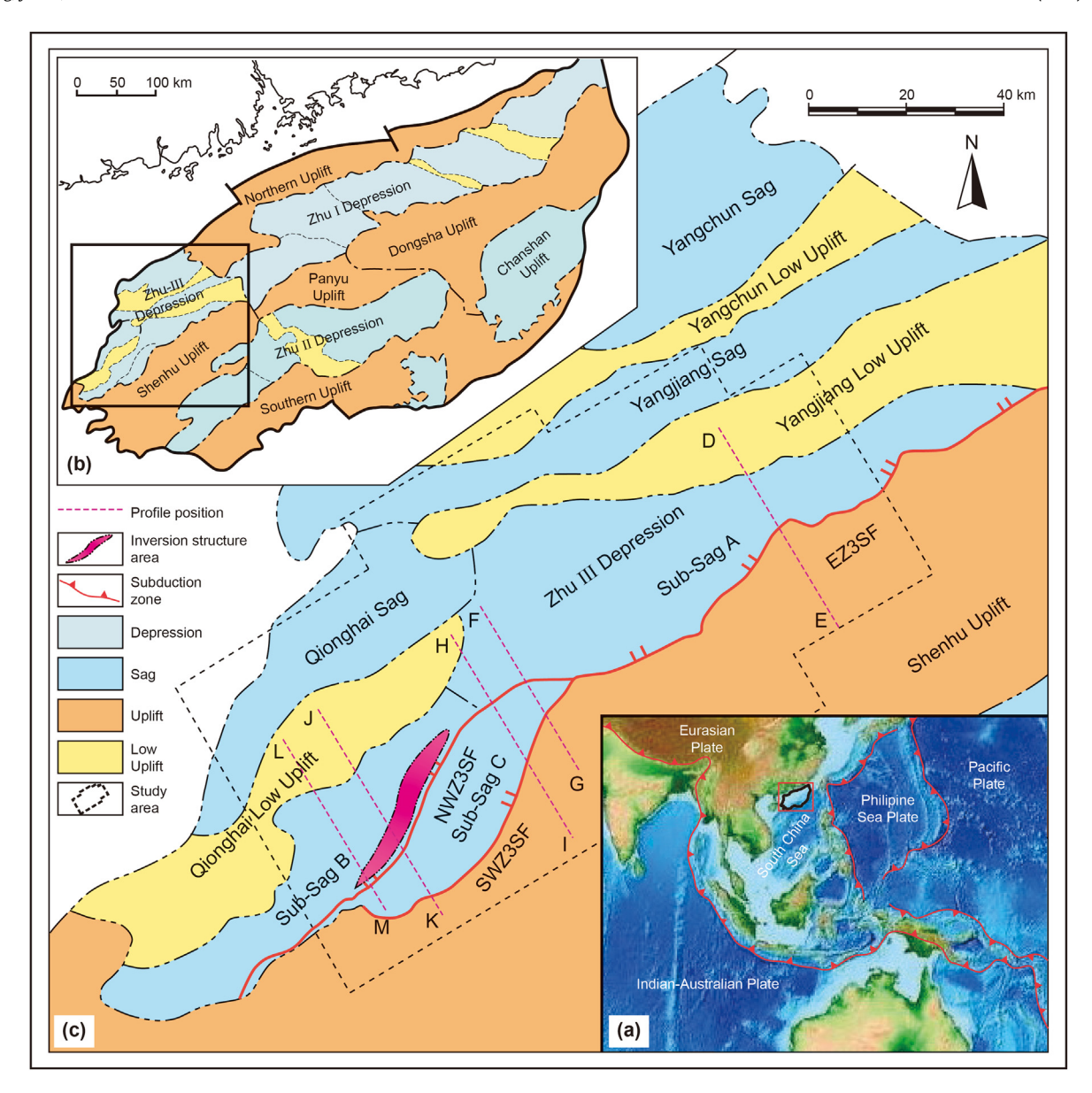


Fig. 1. (a) Sketch map represents the location of the PRMB in the northern SCS margin. The red tooth lines indicate the boundary of Indo-Australia Plate, Eurasian Plate, Philippine Sea Plate and Pacific Plate. Image derived from Google Earth. (b) Map of the subdivisions of tectonic units of the PRMB (modified from Zhu and Mi, 2011). (c) The enlarged map depict the sub-sags and bulges in the Zhu III depression (modified from Zhong et al., 2018). The purple dotted lines are the locations of the Seismic profiles (Figs. 3 and 4). EZ3SF, NWZ3SF and SWZ3SF represent the East Part, the North Branch and South Branch of West Part of the Zhu III South Fault, respectively.

Shenhu, Wenchang, and Enping Formations from the Paleocene to the Eocene. This suggests that the direction of the regional tensile stress was deflected (Ru and Pigott, 1986; Li et al., 1993; Zhou et al., 1995; He et al., 2012). However, there is a paucity of direct proof of the change in the regional tensile stress direction in the basin after the Eocene, especially evidence of the change in the strike of the growth faults in each stratum in the basin about the regional stress direction.

The Wenchang Sag is located in the western part of the PRMB (Fig. 1b and c), and it consists of Wenchang sub-sag A, Wenchang sub-sag B, and Wenchang sub-sag C (referred to as sub-sags A, B, and C in this paper), Yangjiang Low Bulge, and Qionghai Bulge (Huang et al., 2003; Xiao et al., 2009; Cheng et al., 2013; Liu et al., 2022). In the Wenchang Sag, multiple prior studies on the Zhu III South Fault, a boundary fault, focused on the issue of its right-lateral strike-slip motion (Zhang et al., 2013; Jiang et al., 2020).

Abundant studies have reported that the stress condition and preexisting structural configurations significantly influence the strikeslip deformation (Naylor et al., 1986; Schlische et al., 2002; Hsiao et al., 2004; Cunningham and Mann, 2007; Ghosh and Chattopadhyay, 2008; Mitra and Paul, 2011; Dooley and Schreurs, 2012). The strike-slip movement formed a restraining bend and releasing bend at the bending portions of the pre-existing fault (Woodcock and Fischer, 1986; Allen and Allen, 1990; Cunningham and Mann, 2007). The former bend can lead to the formation of positive relief, such as compressional anticlines or uplifts, while the latter can lead to the formation of negative relief, such as extensional sags or a pull-apart basin (McClay and Bonora, 2001; Woodcock, 2003; Cembrano et al., 2005; Mitra and Paul, 2011; Robson et al., 2018). However, there is limited research on the period and timing of the strike-slip activity on the Zhu III South Fault, and the influences of the releasing bend and restraining bend

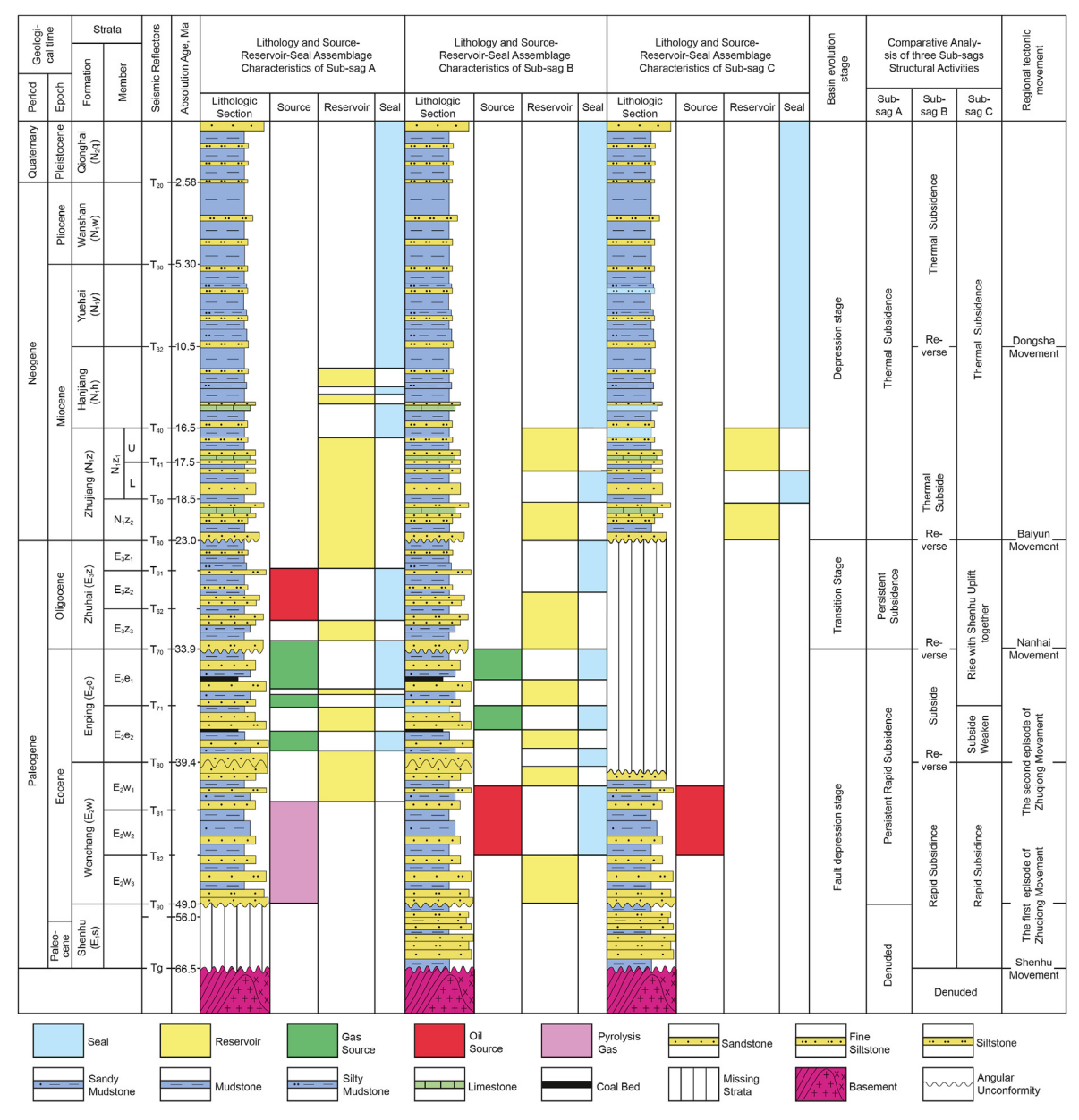
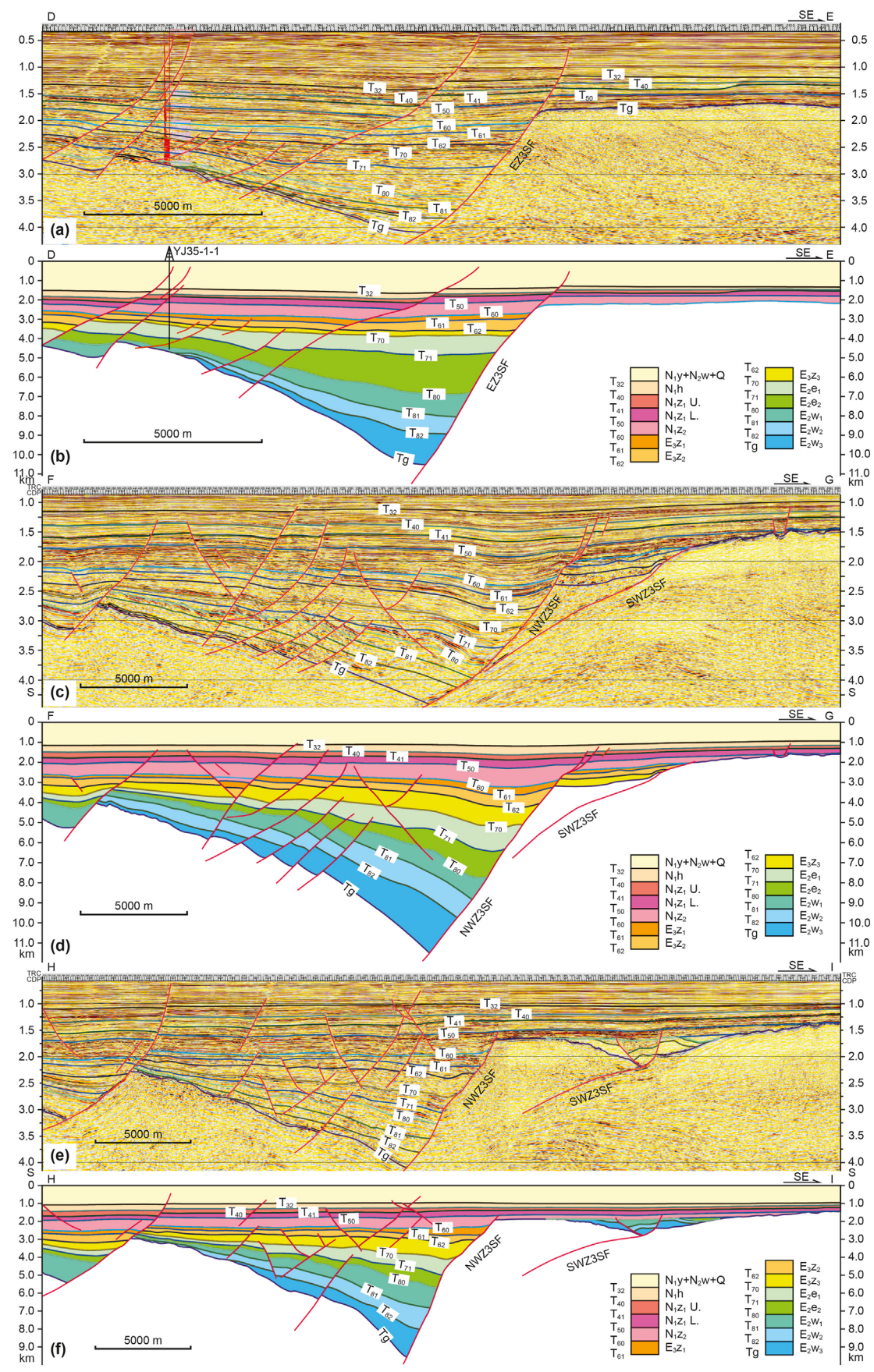


Fig. 2. Feature map of stratigraphic and tectonic evolution as well as the source-reservoir-seal combination of Wenchang A, B, and C sub-sags in Zhu III Depression in the PRMB.

formed via strike-slip movement on the structural deformation in the sag.

Sub-sags A, B, and C are located in the downthrown side of the Zhu III South Fault. The results of several previous studies have shown that there are differences among the three sub-sags, and they have entirely different subsidence histories, deformation characteristics, and regularities in the distribution of the oil and gas (Jiang et al., 2008, 2020; Deng et al., 2012; Gan et al., 2012; Miao et al., 2013; Zhang et al., 2013; C. Li et al., 2014, 2015). However, less attention has been devoted to providing a reasonable explanation for the structural differences of the three sub-sags, the geological period of the structural inversion and the number of structural inversions in sub-sag B.

In order to explain the formation and evolution mechanism of the Wenchang Sag and the causes of the obvious differences in the structures, sedimentation, and hydrocarbon accumulation in the three sub-sags, we studied the differential development history and the characteristics of the structural features of these three sub-sags through interpretation of seismic data, structural mapping, equilibrium profiles, paleogeomorphic restoration, and mechanical analysis. The stress rotation analyzed in this study led to strike-slip movement on the pre-existing normal boundary fault and the formation of a releasing bend and a restraining bend, which controlled the subsequent tectonic evolutions of three sub-sags in the Wenchang Sag. Such analysis not only facilitates better understanding of the genesis of the differences in the structural geology, including the structural deformation, subsidence history, stratigraphic distribution, and oil-gas distribution in the three sub-sags in the Wenchang Sag, but it also provides new insights for the tectonic analysis of similar basins.



**Fig. 3.** Map of seismic profiles interpretation and geological profiles in Wenchang A sub-sag. (a) Seismic profile interpretation of line D–E. (b) Geological profile of line D–E, (c) Seismic profile interpretation of line H–I. (f) Geological profile of line H–I. EZ3SF, NWZ3SF and SWZ3SF represent the East Part, the North Branch of the West Part and the South Branch of the West Part of the Zhu III South Fault, respectively.

#### 2. Geological background

The SCS, at the intersection of the Eurasian, Indo-Australian, Pacific, and Philippine Sea Plates (Fig. 1a), comprises a complex geodynamic background with evolutionary tectonic history (Ren et al., 2002; Ingram et al., 2004). The Pearl River Mouth Basin, which covers an area of  $1.75 \times 10^5 \ \mathrm{km^2}$  (Quan et al., 2015), can be divided into seven sections, including Northern Uplift, Zhu I Depression, Zhu II Depression, Zhu III Depression, Panyu-Dongsha Uplift, Shenhu Uplift, Chaoshan Depression, and Southern Uplift (Zhu and Mi, 2011; Liu et al., 2019) (Fig. 1b). Zhu III South Fault, as the southern boundary of Zhu III depression and Wenchang Sag, is divided into east and west segments. The east part corresponds to the southern boundary fault of sub-sag A, while the west counterpart can be further split into two branches (Fig. 1c). The north and south branches bound the sub-sags B and C, respectively (Lei et al., 2012; You et al., 2018).

The PRMB underwent six tectonic movements that have significant influenced the basin tectonics and sedimentation (Mu et al., 2022). In detail, the Shenhu Movement during the Late Mesozoic (66.5 Ma) is marked by the  $T_{g}$  horizon as a regional unconformity (Li, 1993, Fig. 2). This basin was uplifted and eroded in the first episode of Zhuqiong Movement around Early Eocene (49.0 Ma) (T<sub>90</sub>, Fig. 2), which was also accompanied by magmatic activity. The second phase of the Zhuqiong Movement at around Middle Eocene (39.4 Ma) (T<sub>80</sub>, Fig. 2), additional uplift and erosion are accompanied with faulting and magmatic activities (He et al., 2012). Afterwards, the Nanhai Movement, occurred at Late Eocene (33.9 Ma) and was recorded by a regional unconformity horizon T<sub>70</sub> (Briais et al., 1993; Hutchison, 2004; Hall, 2012) At the same time with these movements, thermal subsidence stages and marine invasion occurred during this phase (Wu, 1984). In the SCS and Southeast Asia, the significant Baiyun Movement (23 Ma) during the Oligocene-Miocene triggered the deep mantle upwelling in Baiyun sag with strong subsidence. In parallel, the Pearl River Delta and correlating deep submarine fan system went through sudden alterations, with the shelf break jumping from the south side of Baiyun sag to the north side (Pang et al., 2009). To Late Miocene (10.5 Ma), the Dongsha Movement took place and induced a regional unconformity T<sub>32</sub> with block rising-and-falling, local contraction, faulting, and magmatic activities (Zhao et al., 2012; Xie et al., 2017). This movement corresponds to the T<sub>32</sub> surface of regional unconformity. Later then, Nansha Movement occurred in 16.5 Ma (Rangin et al., 1990; Hall et al., 2008), with more substantial impacts on the southern basins of the SCS (Madon et al., 2013; Zhang et al., 2020) than that in the PRMB.

Sub-sags A and B are proven to be hydrocarbon-generating sags, with the deposition (Fig. 2) of Wenchang ( $E_2w$ ) and Enping ( $E_2e$ ) Formations during the Eocene, Zhuhai Formations ( $E_3z$ ) during the Oligocene, Zhujiang ( $N_1z$ ), Hanjiang ( $N_1h$ ) and Yuehai Formations ( $N_1y$ ) during the Miocene, and Wanshan Formation during the Pliocene ( $N_2w$ ), as well as Quaternary (Q). Nevertheless, the differences are that deposition of the Shenhu Formation ( $E_1s$ ) appeared in sub-sags B and C rather than in sub-sag A.

## 3. Data and methods

The study area in the Wenchang Sag includes an 8000 km² area with three-dimensional seismic data (Fig. 1c). The drilling wells in the investigated area were exhaustively studied using data from cores and logging curves. After comparing the stratigraphic sequences in the wells, well-to-seismic integration, and mutual calibration, the interpretation scheme for the seismic data was determined.

A sequence stratigraphy framework was established according to the sequence stratigraphy model created by Vail and Posamentier (1988) from Exxon Mobil Corporation. The sequence interfaces were characterized and delineated from four perspectives: (a) the seismic reflection characteristics on the seismic profile (shape, internal structure, top-bottom contact relationship, amplitude, and continuity); (b) lithologic changes, associations, and cycles; (c) identification marks on the logging curves (e.g., amplitude and morphological characteristics of the natural gamma ray, spontaneous potential, and acoustic logging curves); and (d) the age, nature, and intensity of the regional tectonic events.

By projecting the results of the sequence division onto the drilling column section and onto the well-connected seismic section, the sequence interface of the seismic section was identified and divided. The division results were compared and adjusted to make them entirely unified, and the geological significance of the sequence interface was evident. Subordinately, the horizon tracking of a single well-crossing the backbone seismic profile was carried out, and finally, the ten profiles that had been tracked and closed were taken as the basic framework for the seismic interpretation of the entire region.

Fourteen interpretation horizons were defined:  $T_g$ ,  $T_{90}$ ,  $T_{82}$ ,  $T_{81}$ ,  $T_{80}$ ,  $T_{71}$ ,  $T_{70}$ ,  $T_{62}$ ,  $T_{61}$ ,  $T_{60}$ ,  $T_{50}$ ,  $T_{41}$ ,  $T_{40}$  and  $T_{32}$  (Fig. 2). Specifically,  $T_g$ ,  $T_{90}$ ,  $T_{80}$ ,  $T_{70}$ ,  $T_{60}$ ,  $T_{40}$  and  $T_{32}$  are the seismic reflection interfaces of the second-order sequences, which have a large range of unconformity and sedimentary discontinuity and coincide with the boundaries of the formations (Fig. 2).  $T_{82}$ ,  $T_{81}$ ,  $T_{71}$ ,  $T_{62}$ ,  $T_{61}$ ,  $T_{50}$ , and  $T_{41}$  are the seismic reflection interfaces of the third-order sequences, which have a smaller range of unconformity and sedimentary discontinuity and correspond to the boundaries of the members within the formations (Fig. 2).

The geological profile was established by utilizing the interpreted seismic profile and drilling speed data, and the evolution profile of the investigated area was obtained using the backstripping technique. Based on the faults throughout twelve horizons (i.e., T<sub>g</sub>-T<sub>40</sub>), the fault distribution map of each horizon was created. If the thickness of the equivalent layer in the upthrown and downthrown side of a fault was equal, the fault was regarded to be epigenetic rather than growth fault, and the seismic interpretation profile of each fault was examined accordingly. After removing the epigenetic faults from the fault distribution map of the corresponding layer, we counted the number of faults and compared their trends of faults in each horizon. Additionally, the Golden Software Grapher was used to create a rose diagram of the fault trends, and we analyzed the direction of the stress field in the different periods in combination with the regional geologic background.

In order to assess the characteristics of the activity on the main faults, it was necessary to use three-dimensional geological modeling software and to consider the key factors controlling the structure and shape of the sag, which are as follows: (a) the key factors controlling the structure and shape of the sag, such as the distribution and activity of the main faults in the different geological periods; (b) the sedimentary evolution of the basin; and (c) the spatial distribution of the thickness of each horizon. Moreover, in order to restore the distribution characteristics of the paleogeomorphology of this area, several controlling factors were integrated, such as the range of the uplift and erosion area, the recovery of erosion, and the thickness of the sedimentary strata. On the paleogeomorphologic map, the positive color code indicates the height of the uplift-erosion area surrounding the sag, while the negative color code indicates the depth of the paleogeomorphology in the sag. In this study, the locations of the thickest parts of strata were regarded as the depocenters of the sags in the study area.

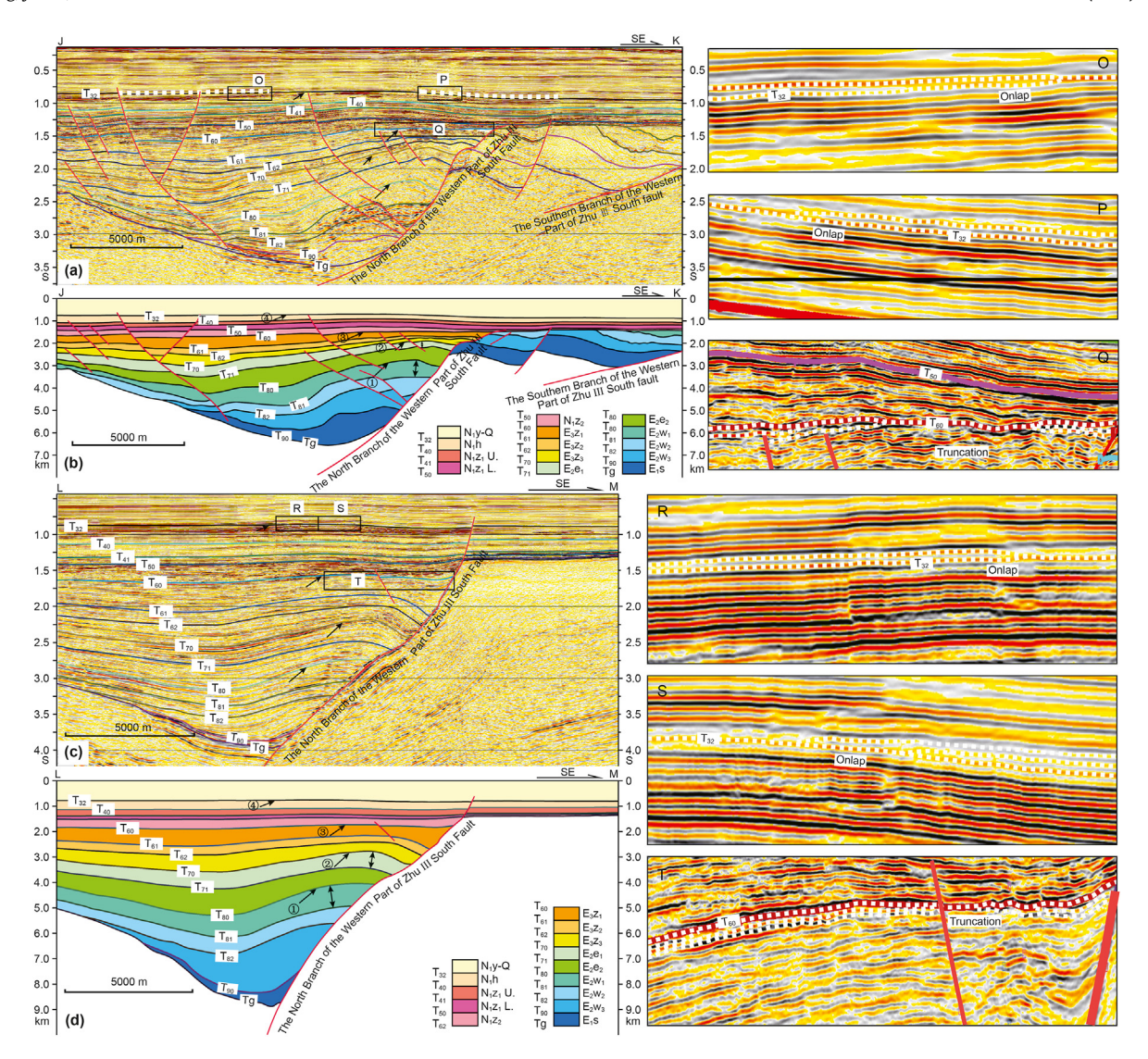


Fig. 4. Seismic profile interpretation and geological profiles in Wenchang B sub-sag. (a) Seismic profile interpretation of line J−K. (b) Geological profile of line J−K. (c) Seismic profile interpretation of line L−M. (d) Geological profile of line L−M (see Fig. 1c for the section position; the arrows indicate the inversion strata and ⊙—⊙ indicate the number of inversion periods while the double arrows illustrate the fold arch-up at the position with greater thickness). The right images marked with O, P, Q, R, S and T are magnified version of the seismic profile of J−K and L−M in the left corresponding to the range delineated by black boxes with labels of O, P, Q, R, S and T respectively.

#### 4. Results

### 4.1. Strata, structure, and variations

Sub-sags B and C formed earlier than sub-sag A. This was inferred from the fact that the Shenhu Formation, the oldest strata, is present in sub-sags B and C but is absent in sub-sag A (Figs. 2–4). The Wenchang Formation and the strata above it were fully developed in sub-sags A and B. In contrast, part of the elevated Wenchang Formation in the sub-sag C were eroded with omission of the Enping and Zhuhai Formations (Figs. 2–4).

Sub-sag A differs from the adjacent sub-sags in that it has undergone continuous subsidence, with a maximum subsidence thickness of over 10,000 m (Fig. 3). Sub-sags B and C have maximum burial depths of ~8000 m and ~4000 m, respectively (Li et al., 2014). In the late stages of the sedimentation of the first member of the Wenchang Formation, the strata of the syn-rift were eroded more strongly in sub-sag C (Fig. 4a and b).

The development of an inversion structure, which is a significant structural feature, was identified in sub-sag B, whereas sub-

sag A does not contain this structure. The interpretation of the seismic sections (Fig. 4) and the back-stripping analysis conducted in this study revealed that four structural inversions have occurred in sub-sag B (denoted by the arrows and numbered  $\oplus - \oplus$  in Fig. 4b, d), indicating that its evolution was characterized by multiple alterations, such as stretching-inversion-restretching-reinversion.

The first structural inversion occurred in the last depositional period of Wenchang Formation during the Middle Eocene ( $T_{80}$ ). The Shenhu and Wenchang Formations on the downthrown side of the North Branch of the West Part of the Zhu III South Fault were uplifted and compressed in sub-sag B, where the strata were bent and arched up, leading to a bulge in the thickest part of the strata (denoted by the double arrows in Fig. 4b, d). This feature was observed within the first member of the Wenchang Formation, i.e.,  $T_{81}-T_{80}$  (Fig. 4a, d). After the first structural inversion, the depocenter migrated northward and away from the North Branch of the West Part of the Zhu III South Fault. Due to the leveling-up and filling sedimentary processes, the strata above the inversion of the stratigraphy tend to be thin at the top and thick in the limbs, which is illustrated within the second member of the Enping Formation

(i.e., T<sub>80</sub>-T<sub>71</sub>) in Fig. 4b.

The second structural inversion in sub-sag B occurred in the last depositional period of Enping Formation during the Late Eocene  $(T_{70})$ . This inversion represented by the bending and uplift of the thickest part of the first member of the Enping Formation  $(T_{71}-T_{70})$  (Fig. 4d). It is more evident on cross-section L-M because there are fewer minor faults (denoted by the double arrows in Fig. 4c, d). Subsequently, all of the members of the Zhuhai Formation, including the third  $(T_{70}-T_{62})$ , second  $(T_{62}-T_{61})$ , and first  $(T_{61}-T_{60})$  members of the Zhuhai Formation, exhibit thin tops and thick limbs in the cross-section.

In addition, the third structural inversion in sub-sag B occurred in the terminal depositional period of Zhuhai Formation ( $T_{60}$ ), and there is conspicuous unconformity at the top. Due to strong erosion, truncation occurred (illustrated in the local zoomed in sections of images Q and T in Fig. 4), indicating that the crucial inversion and erosion occurred simultaneously. The lack of significant onlap above this surface suggests that the paleotopography did not fluctuate much after the top was eroded. The thin top and thick limbs of the second member of the Zhujiang Formation ( $T_{60}$ – $T_{50}$ ) further demonstrate the occurrence of reversion and arching-up in the final depositional period of Zhuhai Formation ( $T_{50}$ – $T_{32}$ ), there is no horizontal change in the thickness of the strata, suggesting that the filling and leveling-up depositional processes have been completed by this time.

The fourth structural inversion in sub-sag B occurred in the late depositional period of Hanjiang Formation during the Middle Miocene. The interface, namely,  $T_{32}$ , arched up, and the onlap layers above the exposed part occurred (illustrated in the enlarged parts marked as O, P, R, and S in Fig. 4). No truncation was observed beneath the strata interface  $(T_{32})$ , whereas the onlap strata were observed above the interface  $(T_{32})$ .

#### 4.2. Strikes of growth faults

The change in the strikes of the growth faults identified on the rose diagram may reveal variations in the direction of the regional tensile stress over time. Fourteen sequence interfaces in this region were interpreted, and planar combination was conducted on the growth faults in the twelve interfaces in order to analyze the differences in the direction of the regional tensile stress during the various periods of the Wenchang Sag (Fig. 5).

In addition, a rose diagram of the fault strikes was created using the layered statistics of the strikes of the growth faults with lengths of more than 4 km. Specifically, comparison of surfaces  $T_g$  to  $T_{40}$  suggests that in the bottom of Shenhu Formation (i.e.,  $T_g$ ), there are NNE trending faults (Fig. 5a). In addition to the features of the faults in the Shenhu Formation, particular examples of the strikes of the faults in the Wenchang, Zhuhai and Enping Formations in the study area are described in the next paragraph.

As can be seen from Fig. 5b—d, in surfaces of  $T_{82}$ ,  $T_{81}$ , and  $T_{80}$ , there are faults in two directions on the rose diagram: one is the strike of the fault within the sag, and the other is the strike of the boundary fault of the sag. Since there are few concave faults, the boundary faults exhibit only one dominant direction on the rose diagram. The noticeable increase in the number of faults within the sag, which have a preponderance of orientations and signify the direction of the regional tensile stress, would cause the boundary faults to be omitted from the rose diagram. For example, surface  $T_{82}$ , at the top of the third member of the Wenchang Formation, is characterized by primarily NE-trending faults (Fig. 5b). The majority of the faults in surface  $T_{81}$  are NEE-trending (Fig. 5c). At the very top of the Wenchang Formation, the faults in surface  $T_{80}$  are roughly E-W-trending (Fig. 5d).

As can be seen from Fig. 5e–l, the rose diagrams only display one primary direction, since the boundary faults are not readily apparent on the rose diagrams when there are multiple faults in eight surfaces, such as  $T_{71}$ ,  $T_{70}$ ,  $T_{62}$ ,  $T_{61}$ ,  $T_{60}$ ,  $T_{50}$ ,  $T_{41}$ , and  $T_{40}$  in the sag. In detail, the strikes of the faults in surfaces  $T_{71}$ ,  $T_{70}$ ,  $T_{62}$ ,  $T_{61}$ , and  $T_{60}$  are E-W-trending, whereas the faults in surfaces  $T_{50}$ ,  $T_{41}$ , and  $T_{40}$  are NEE-trending.

#### 4.3. Paleostress analysis

According to the Anderson model (Anderson, 1951) and the fault distribution model (McClay and Ellis, 1987; McClay, 1990; Acocella et al., 2000; Contreras et al., 2000; Peacock, 2002; Patton, 2005), the strike of a normal fault is perpendicular to the direction of the regional tensile stress. The pre-existing faults have an effect on the newly formed faults. Additionally, a new fault that forms in an area distant from the original basement fault has a strike that is nearly perpendicular to the direction of the regional tensile stress (Tong, 2010).

This directional linkage is illustrated in Fig. 5. The characteristics of the tensile stress are as follows: (1) The WNW-trending features may occur on surface  $T_g$ , the bottom of the Shenhu Formation. (2) The tensile stress is oriented northwest at the top of the third member of the Wenchang Formation (i.e.,  $T_{82}$ ) and NNW at the top of the second member of the Wenchang Formation (i.e.  $T_{81}$ ). (3) Surfaces  $T_{80}$ ,  $T_{71}$ ,  $T_{70}$ ,  $T_{62}$ ,  $T_{61}$ , and  $T_{60}$ , all exhibit nearly N-Strending tensile stress, while surfaces  $T_{50}$ ,  $T_{41}$ , and  $T_{40}$ , all exhibit a NNE-trending stress (Fig. 5).

The trends of the faulted basin during the various phases in the PRMB can be used to confirm the change in the orientation of the regional tensile stress. The trend of the faulted depressions, which was filled with the Shenhu Formation throughout the Paleocene, was from NNE to NE (Li, 1993), suggesting that the direction of the regional tensile stress changed from WNW-ESE to NW-SE during this period. During the Middle Eocene, the trend of the fault depression that was filled with the Wenchang Formation, was NE-NEE (Zhou et al., 1995), which seems to imply that the regional tensile stress changed from NW-SE to NNW-SSE during this period. Furthermore, during the Late Eocene, the faulted depressions, which were completely filled by the Enping Formation, was roughly E-W-trending (He et al., 2012), demonstrating that the regional extending stress was oriented nearly S-N. The evidence presented above supports the conclusion drawn from the rose diagram of the growth faults in the different horizons.

#### 5. Discussion

## 5.1. Causes of variations and differences in the three sub-sags

In studies of the three sub-sags, the determination of the change in the direction of the regional tensile stress associated with each tectonic phase is significant, since it may have enabled the production of a strike-slip component in the pre-existing boundary fault. The direction of the regional tensile stress rotated clockwise from NNW-SSE, to NW-SE, to NNW-SSE, to near S-N and to NNE-SSW (Figs. 5 and 6). When the direction of the tensile stress changed to NW-SE-trending, the extension was dominant, because this trend was roughly perpendicular to the overall extension direction of the Zhu III South Fault, and no strike-slip component was generated.

When the direction changed to NNW-SSE or nearly S-N or NNE-SSW-trending, the inclination of the regional tensile stress intersected with the general extension direction of the Zhu III South Fault at an acute angle, generating strike-slip stress in the direction parallel to the Zhu III South Fault. As the Zhu III South Fault was arc-

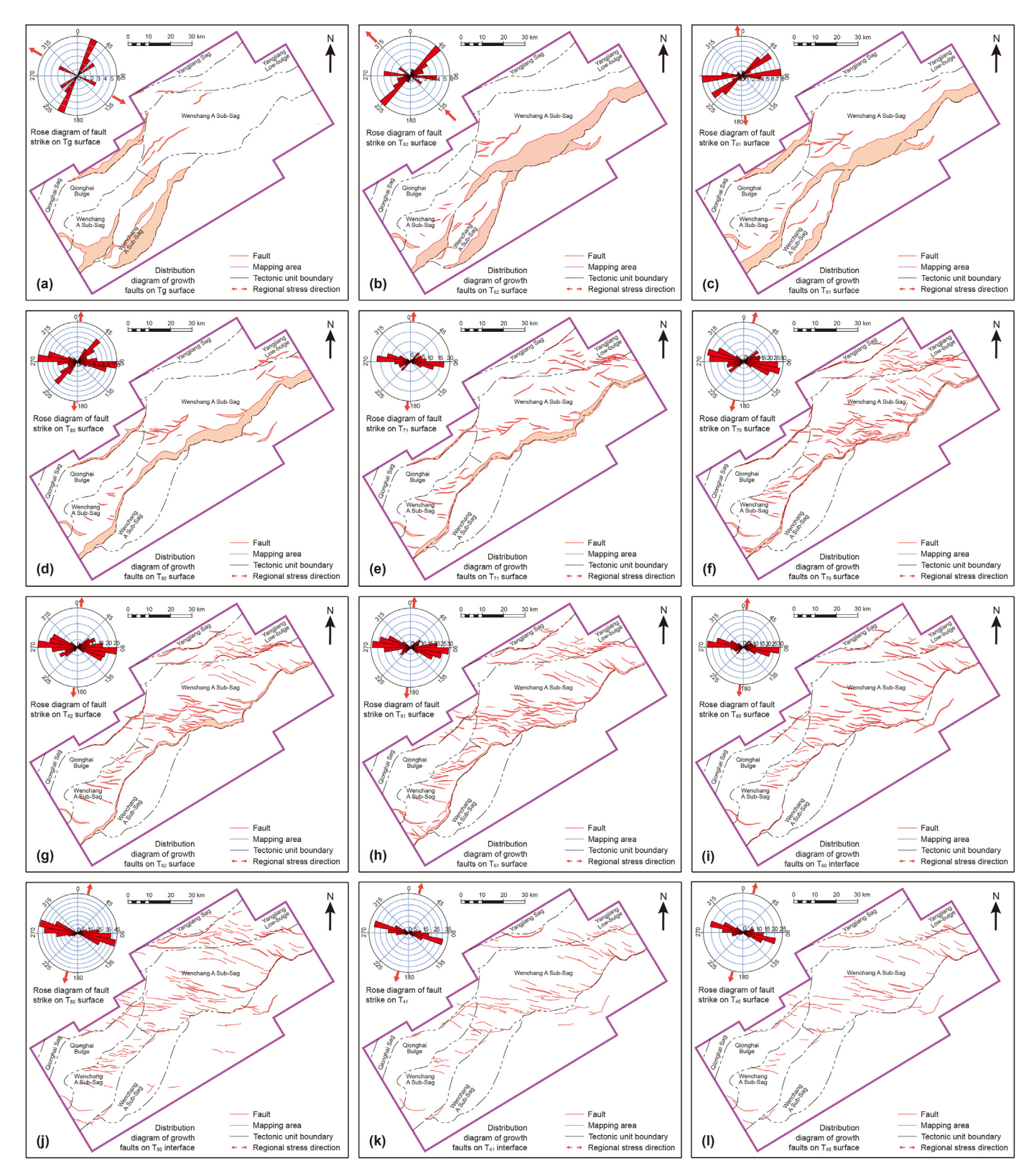


Fig. 5. Distribution map of the growth faults (the center of the map) and rose diagram (the upper left corner of the map) of the strikes of the growth faults at different reflecting layers in Wenchang Sag. A set of data near the horizontal axis in each rose diagram represent the number of counted faults.

shaped in the plane, this strike-slip component contributed significantly to the development of the inversion structures in the sub-sag B in the restraining bend of the North Branch of the West Part of the Zhu III South Fault. The strike-slip stress increased as the clockwise deflection angle of the tensile stress became larger. The pull-apart subsidence in the sub-sag A near the East Part of the Zhu

III South Fault was also caused by the strike-slip stress. As a result, structural inversion did not occur in sub-sag A, but it did occur in sub-sag B. Instead, sub-sag A experienced pull-apart subsidence, suggesting a high degree of linkage with its persistent subsidence. The interpreted pressurization mechanism of sub-sag C was similar to that of sub-sag B. However, the local contraction and uplift were more significant in sub-sag C and acted as the double restraining bend, due to the influence of the South Branch and North Branch of the West Part of the Zhu III South Fault (Fig. 6).

When sub-sag B underwent pronounced inversion and sub-sag C experienced strong uplift and erosion, the deposition rate of the Enping Formation in sub-sag A increased to the greatest level (Gan et al., 2014). This suggests that the inversion structure in sub-sag B and the uplift and atrophy in sub-sag C, were produced by local contraction in the restraining bend of the Zhu III South Fault, rather than by the change in the regional stress from extension to compression. The strike-slip component parallel to the Zhu III South Fault, is speculated to have most likely been activated by the rotation of the regional tensile stress direction.

Based on the interpretations and results presented the previous sections, the West Part of the Zhu III South Fault, the earliest faults, originated due to the WNW-trending extension during Shenhu Movement in the Early Paleocene (Fig. 2). The strata of the Shenfu Formation are only distributed on the downthrown side of the West Part of the Zhu III South Fault (Fig. 7). Among the six tectonic movements in the northern margin of the SCS, Shenhu Movement was the initial rift activity and thus, Cenozoic sediments were not deposited. As a result, it was impossible for this movement to cause structural inversion.

The first episode of Zhuqiong Movement occurred during the Early Eocene. The extension direction was NW-SE, and the East Part of the Zhu III South Fault formed. As the tensile stress direction was oriented NW-SE, it was perpendicular to the strike of the Zhu III South Fault. Due to the absence of strike-slip components parallel to the Zhu III South Fault during the aforementioned tectonic movements, it can be further speculated that neither a restraining bend nor a releasing bend formed. Consequently, sub-sag B did not undergo any noticeable structural inversion.

As depicted in cross-section J–K in Fig. 4, the thickness of the Shenhu Formation and the third member of the Wenchang Formation are comparable to those of the homologous strata in subsag B. This implies that the present sub-sag B and sub-sag C were once a unified sag (Fig. 7). Sub-sags B and C, with the subsidence center located in sub-sag C, were situated on the downthrown side of the South Branch of the West Part of the Zhu III South Fault during deposition of Wenchang and Shenhu Formations. The North Branch was formed later than the South Branch and divided into two disconnected sections (Fig. 8a, b). The East Part of the Zhu III South Fault formed in the Middle Eocene, and sub-sag A started to receive the deposition of the Wenchang Formation (Fig. 8c, d).

In the late depositional period of Wenchang Formation, the second episode of Zhuqiong Movement occurred. The direction of the regional tensile stress significantly shifted from NNW-SSE to nearly S-N. The intersection between the tensile stress direction and the trend of the Zhu III South Fault was oblique, generating a strike-slip component parallel to Zhu III South Fault (Fig. 6). The architecture of sub-sag B was noticeably inverted, and sub-sag C atrophied via compression and uplift. The most noticeable characteristics of the structural inversion are the upward arching and uplift of the thickest portion of the strata, which is a reliable feature for the identification of structural inversion. The formation mechanism is shown in Fig. 9. The top and bottom surfaces of the strata protruded, with a large curvature at the top and minor curvature at the bottom (Figs. 9-1b). In addition, sub-sag A continuously subsided to a large depth (Fig. 8e and f). Then, the activity on the South Branch of the West Part of the Zhu III South Fault gradually decreased. Consequently, the activity on the West Part of the Zhu III South Fault was mainly concentrated in its northern branch (Fig. 7).

During the deposition of the second member of the Enping Formation, the South Branch of the West Part of the Zhu III South Fault was basically inactive. Sub-sag C suffered local compression in the arcual portion of the South Branch of the West Part of the Zhu III South Fault and formed folds, which were uplifted with the Shenhu Uplift and were eroded as a whole, leading to the absence of the Enping and Zhuhai Formations. In addition, folds formed in the Shenhu and Wenchang Formations as a result of the local compression in the arcual portion of the fault (Fig. 3e and f and Fig. 4a and b). Until the depression stage, thermal subsidence occurred in sub-sag C, and it started to receive the sediments of Zhujiang Formation. Therefore, although the Shenhu and Wenchang Formations developed in sub-sag C, the Wenchang Formation was partially eroded and the Enping and Zhuhai Formations were completely eroded away (Fig. 4b). During the depositional period of Zhuhai Formation, the regional tectonic stress was orientated NNE with a large deflection. The bottom (T<sub>70</sub>) and top (T<sub>60</sub>) surfaces of Zhuhai Formation coincide with the Nanhai and Baiyun Movements, respectively. During these two tectonic movements, due to the greater regional tensile stress, the strikeslip component along the Zhu III South Fault was stronger, resulting in obvious structural inversion in sub-sag B (Figs. 4 and 7) and uplift of the entirety of sub-sag C (Fig. 8g, h). The characteristics of the inversion structures on surface  $T_{70}$  are similar to those on surface T<sub>80</sub> (Figs. 9-1a-1c)). The formation process and mechanism of the inversion structures on surface T<sub>60</sub> are portrayed in Figs. 9-2a-2c.

Although the general tectonic stress persisted in the NNE direction during the deposition of the Zhujiang Formation, the Wenchang Sag entered a phase of overall regional subsidence, and the horizontal tensile strain was small. The intensity of the activity on the boundary fault dramatically decreased, and the North Branch of the West Part of the Zhu III South Fault was basically inactive (Fig. 7). Subsequently, overall regional subsidence was initiated. Due to these factors, the influence of the boundary fault on sedimentation decreased. The extent of the transgression

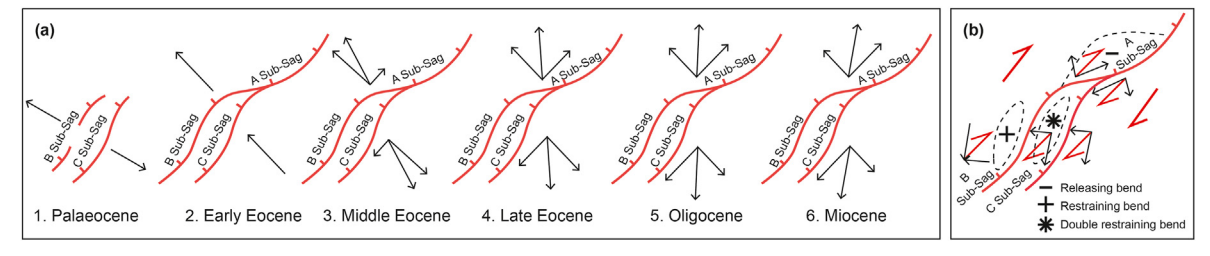


Fig. 6. Mechanical analysis diagram. (a) Schematic diagram of strike-slip stress in the Zhu III South Fault generated by the direction change of regional tensile stress. (b) Schematic diagram of the pull-apart and contraction effects at different parts of the arcuate fault owing to its strike-slip.

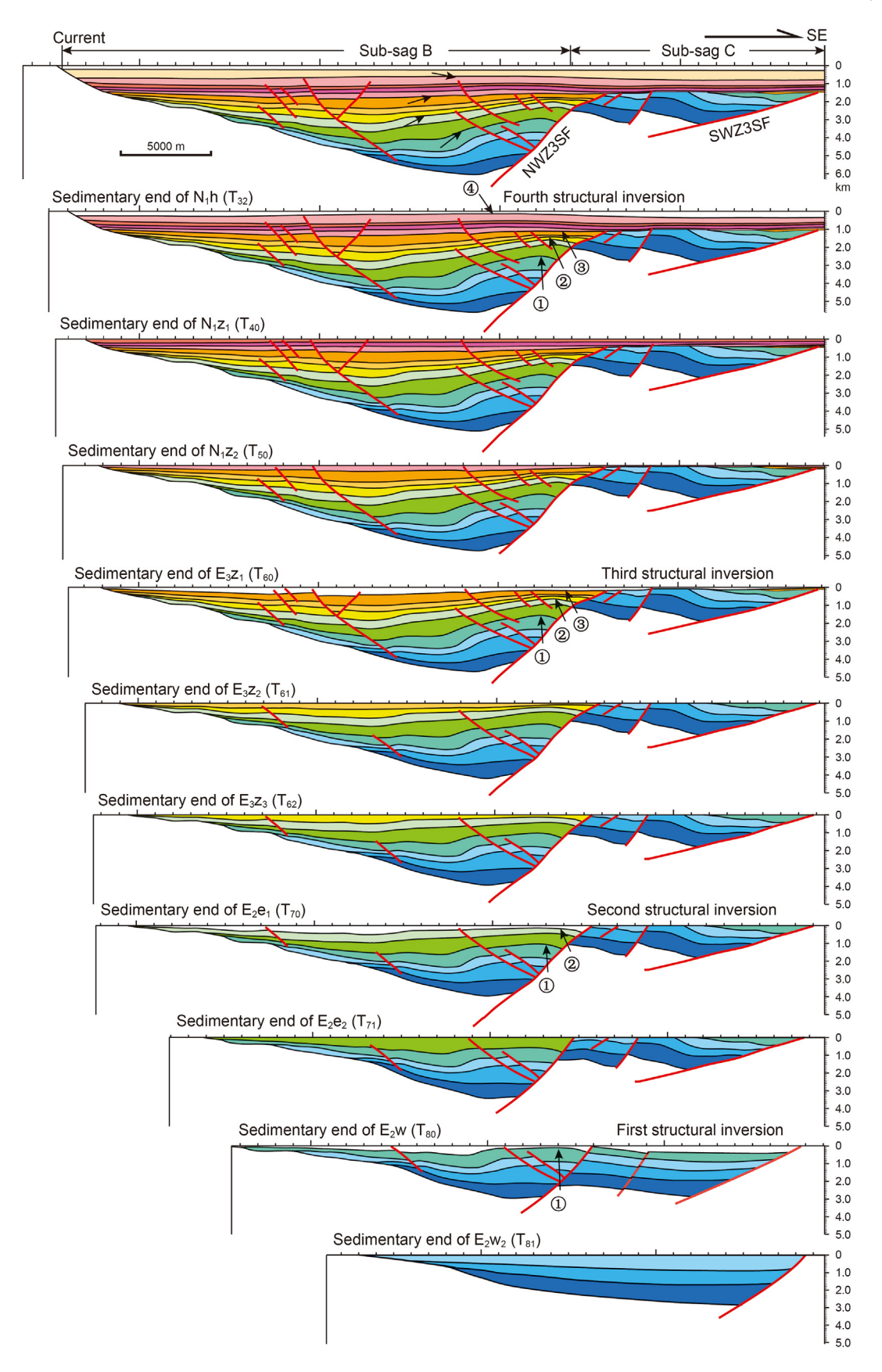


Fig. 7. Tectonic evolution profile of line J—K in sub-sag B and sub-sag C (see Fig. 1c for the section position; the arrows indicate the inversion stratum and ①—④ indicate the number of inversion periods. NWZ3SF and SWZ3SF represent the North and South Branches of the West Part of Zhu III South Fault).

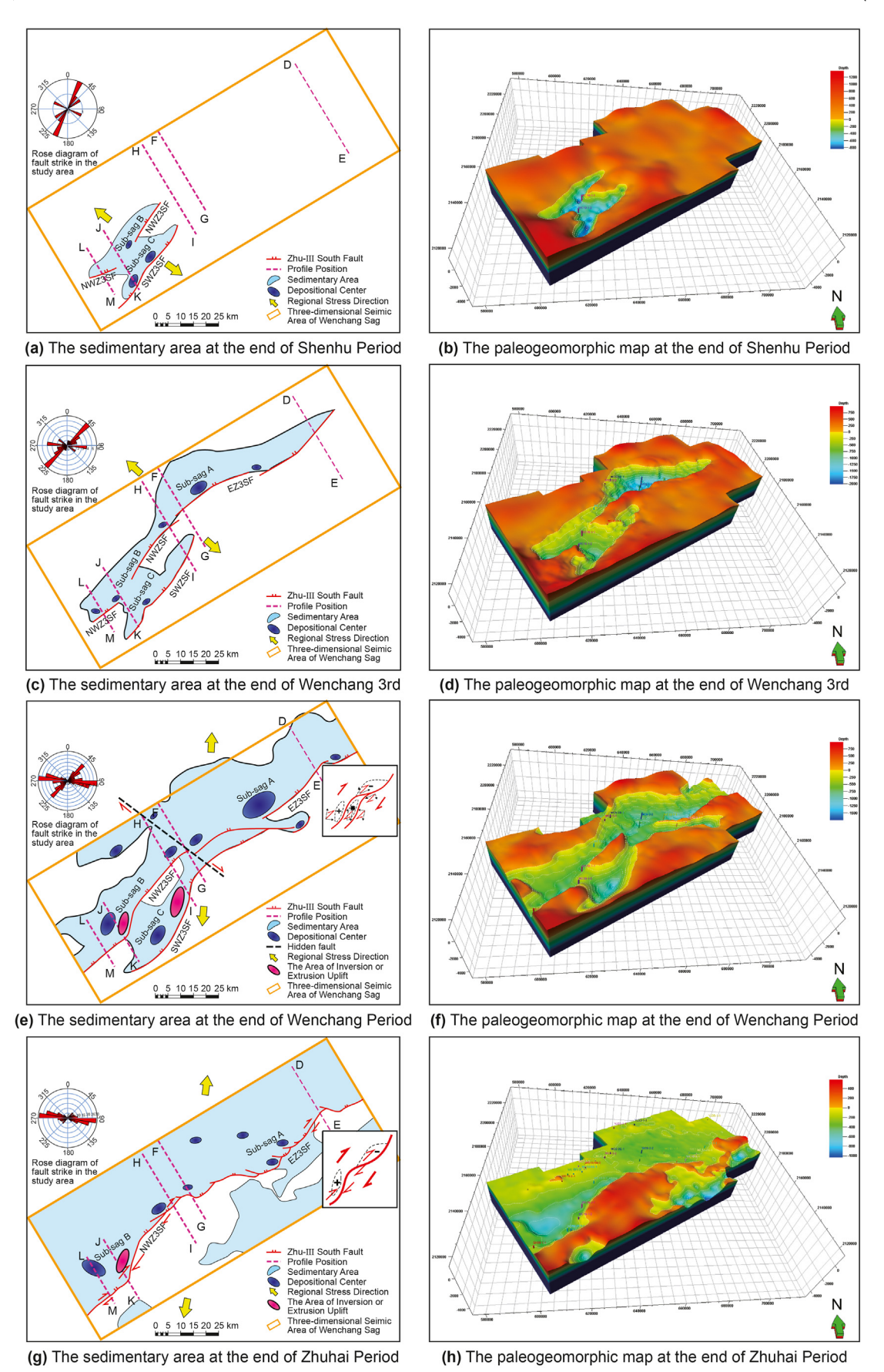


Fig. 8. Schematic (left) and paleogeomorphic map (right) and distribution of the main faults and sedimentary range at different time in Wenchang Sag. EZ3SF, NWZ3SF and SWZ3SF represent the East Part, the North Branch of the West Part and the South Branch of the Zhu III South Fault, respectively.

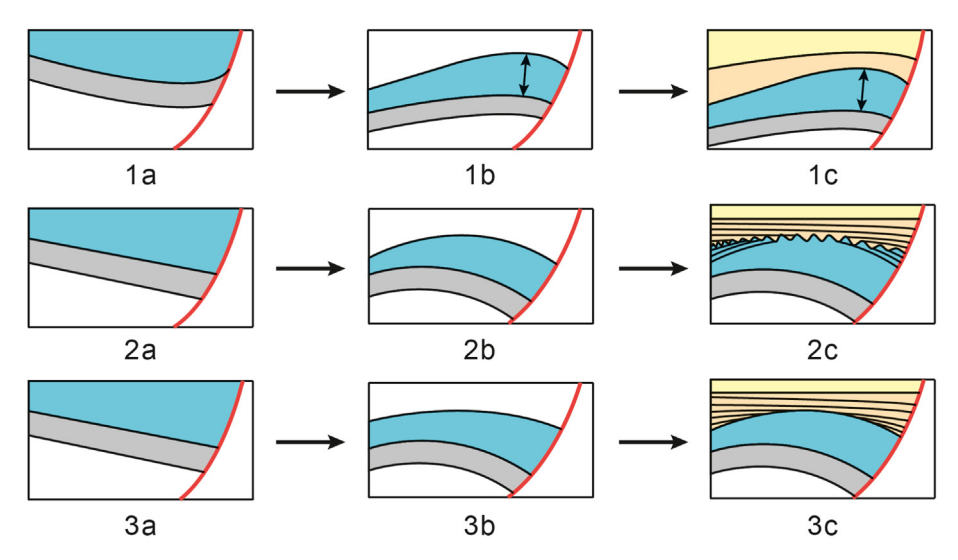


Fig. 9. Schematic diagram of the formation process of inversion structure, 1a–1cThe formation process of the phenomenon of thick top and thin limbs of inversion structure; 2a–2c: The formation process of onlap on unconformity surface of inversion structure; 3a–3c: The formation process of onlap on unconformity surface of inversion structure.

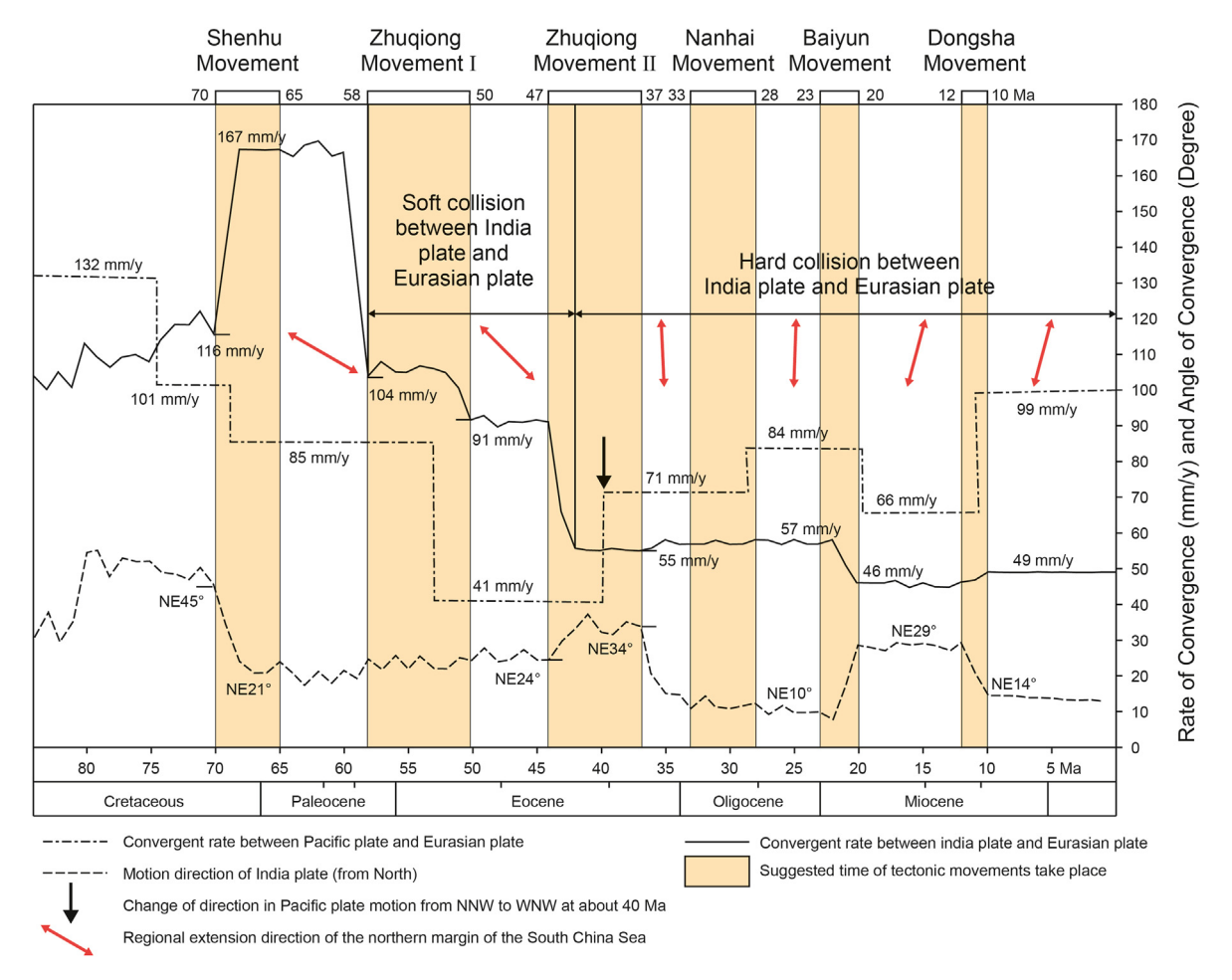


Fig. 10. Map of the convergent rate and direction of India Plate and Pacific Plate relative to Eurasia during the Late Cretaceous and Cenozoic (after Jackson et al., 1975; Lee and Lawer, 1995; Northrup et al., 1995; Van Hinsbergen et al., 2011; Sun et al., 2020).

continuously grew, and the Shenhu and Qionghai Uplifts were rapidly covered by seawater and began to receive sediments. The depocenter of the second member of Zhujiang Formation was located in the middle of sub-sag B. The Qionghai Sag to the north acted as the depocenter of the first member of the Zhujiang Formation. At the end of the deposition of the Wanan Formation  $(T_{32})$ ,

the fourth structural inversion took place and produced a large range of effects (Figs. 4 and 7). The formation process and mechanism are shown in Figs. 9-3a—3c.

Based on the explanation of the mechanism of the differences of three sub-sags in the Wenchang Sag, the four notable structural inversions in sub-sag B indicate that four recognizable periods of dextral strike-slip motion occurred on the Zhu III South Fault, and the timing of the strike-slip motion was consistent with the structural reversion since the structural inversions arose from the strike-slip motion. The occurrence times of the inversion and strike-slip motion are mutually correlated with the four previously mentioned tectonic movements.

#### 5.2. The reasons of stress rotation, geodynamics

In this research, the regional tensile stress is revealed to have a counterclockwise deflection from a WNW-ESE trend in the Early Paleocene to NW-SE and NNW-SSE trends in the Eocene, followed by a roughly N-S trend in the Oligocene, and by a NNE-SSW trend in the Miocene. While, along with similar observation from previous research (He et al., 2012; Jiang et al., 2020), the dynamic mechanism behind deflection is still not clear. To present and compare the development of the regional stress since the Late Cretaceous in detail, the rate and orientation of plates surrounding SCS are plotted in Fig. 10 with highlights on distinct movements, such as the velocity of Pacific plate relative to Eurasia (Northrup et al., 1995), rate and angle of convergence between India and Eurasia plates (Lee and Lawer, 1995) and the transformation of the direction of the Pacific Ocean movement (Jackson et al., 1975; Sun et al., 2020). These previous research suggest a strong correlation between the movements of the three major plates surrounding SCS, and the remarkable tectonic events along the northern South China Sea margin.

From 70 Ma to 65 Ma, a remarkable increase of the convergence rate (from 116 mm/y to 167 mm/y) between the Indian and the Eurasian plates was recorded with a shifted direction from NE45° to 21° (Fig. 10) (Lee and Lawrence, 1995). In parallel, the convergence rate between Pacific and the Eurasian plates was slowed substantially, from 101 to 85 mm/y (Fig. 10), corresponding to the Shenhu Movement (Li, 1993; Cai et al., 2010; He et al., 2012). The motion rate of the Pacific plate has reduced, whereas that of the Indian plate has increased dramatically, which is proposed to result from the steepened and retreated subduction of West Pacific in the Late Cretaceous as well as the onset of large-scale rifting along East Asian continental margin (Li, 1993; Zhou et al., 1995; Guo et al., 2001). Before the collision between the Indian plate and Eurasian plate, the tectonic environment in East Asia was mainly affected by the subduction of the Pacific plate (Zhou et al., 1995; Guo et al., 2001). Since the movement direction of the Pacific plate was WNW-trending during Paleocene, the retreat of the subduction displayed ESE-trending, forming a regional WNW-ESE tensile stress (Northrup et al., 1995).

From 58 Ma to 50 Ma, the first episode of Zhuqiong Movement derived from the decreased convergence rates between both the Indian and Eurasian plates (from 167 to 104 mm/y), and the Pacific and Eurasian plates (from 85 to 41 mm/y) (Fig. 10), as well as a soft collision began between the Indian plate and the Eurasian plate (Lee and Lawer, 1995) and the extrusion of the Indo-Chinese block (Guo et al., 2001). At the same time, the southeastward retreat of Pacific large-angle subduction belt led the East Asian lithosphere to creep in the south-east direction, inducing a regional NW-SE extension in study area.

During the period of 47 Ma-37 Ma, the convergence rate between the Indian and Eurasian plates slowed substantially (from 91 to 55 mm/y) while that between the Pacific and Eurasian plates rose

from 41 to 71 mm/y, in accordance with the second episode of Zhuqiong Movement (Li, 1993; Cai et al., 2010; He et al., 2012). The orientation of this movement, including the Pacific and Indian plates, was significantly altered in this period (Jackson et al., 1975; Sun et al., 2020). In parallel, the hard collision between the Indian and Eurasian plates (Lee and Lawer, 1995) resulted in the Indo-China block being rapidly squeezed out in the southeast direction (Guo et al., 2001). At the same time, the flow of mantle material under the South China plate was nearly N-S-trending, in the same direction with the squirmed northern South China Sea margin (Guo et al., 2001). This could be the precondition for the nearly N-S-trending regional extension within study area.

Along with the Nanhai Movement, from 33 Ma to 28 Ma, the convergence rate between Pacific and Eurasian plates was slightly accelerated from 71 to 84 mm/y, whereas the Indian and Eurasian plates remained steady (Fig. 10) (Lee and Lawer, 1995). At the same time, the result of Indochina block being southeastward squeezed out with clockwise rotation triggered the fact thatthe northern SCS margin stretched in north-south direction (Guo et al., 2001).

The convergence rate of the Indian and Eurasian plates reduced to some extent as the motion direction of the Indian plate (from North) changed from NE10° to NE29° (Lee and Lawer, 1995). Meanwhile, the convergence rate between the Pacific and Eurasian plates was evidently diminished (Fig. 10) (Northrup et al., 1995). These mutations are interlinked and included within the Baiyun movement (Pang et al., 2009).

From the mid-Miocene to Quaternary, the northward subduction of the Indian Ocean-Australian Plate began to dominate the tectonics in study area. Due to the intensifying intraplate deformation (e.g., the rapid rise of the Tibet Plateau) and the opening of the SCS since the Late Oligocene, the influence of the "hard collision" of India and Tibet on the region of the SCS was weakened considerably (Zhou et al., 1995). In parallel, the northward subduction of Indian Ocean-Australian plate and the northwestward shifting and docking of the Philippine Sea Plate became another controlling factor on the tectonic evolution of study area, such as the NNE extension of northern SCS margin after the mid-Miocene.

During Dongsha Movement from 12 Ma to 10 Ma, the convergence rate between Pacific and Eurasian plates increased from 66 to 99 mm/y (Fig. 10) (Northrup et al., 1995) while the angle between these convergence direction and due north decreased (from NE29° to NE14°) (Fig. 10), reducing its effect on the NNE-SE-SW regional expansion.

## 5.3. Significance of oil and gas exploration

The fundamental distinction between the three sub-sags is primarily reflected in the fact that the sub-sag A is a releasing bend superimposed with the subsidence of strike-slip pull-apart, considerable subsidence range and no structural inversion. The source rocks of the Wenchang Formation were over-mature (Quan et al., 2015, 2018) and had entered the pyrolysis stage following subsequent continual sinking (Huang et al., 2003, 2007). Such subsequent continual sinking process also reinforced the thermal evolution of source rocks within the Enping Formation, where competence of hydrocarbon generation was thereby strengthened (Cheng et al., 2013). Thus, the sub-sag A is capable of yielding both gas and oil (Gan et al., 2012; Lu et al., 2016). By contrast, the sub-sag B is located in the restraining bend area, where has experienced four structural inversions with a less subsidence than that in the sub-sag A.

Wenchang Formation, the primary source rock in sub-sag B, has been in its "oil window", maturity stage, since the Oligocene. Conversely, the part of the source rocks of the Enping Formation in the sub-sag B are still immature, as their entrance within the oil-

generating threshold is delayed by the shallower burial (Li et al., 2015). Therefore, the sub-sag B were reported as mainly produces oil by previous studies (Zhang et al., 2009, 2011; Deng et al., 2012; Gan et al., 2012). Except for the aforementioned sub-sags, the Wenchang sub-sag C, because of its location between the double restraining bends of the North Branch and South Branch of the West Part of the Zhu III South Fault, underwent both strong contraction and uplift. While, there is no petroleum reservoir since the Enping Formation and parts of the Wenchang Formation have been eroded and buried at shallow depth (see Li et al., 2022; for examples). Important for this study, the categories of oil and gas traps in sub-sag A include the faulted block and the rollover anticline associated with the growth normal faults, whereas those in sub-sag B contain inversion structures and fault blocks.

Inversion structures, resulting from typical post-sedimentary contraction, usually comprise a relatively large area and height. Meanwhile, the area and height of the rollover anticline are entirely determined by the degree of fault activity. By contrast, the scale of oil and gas fields in the inversion structure of the sub-sag B is greater than that in rollover anticline of the sub-sag A.

Moreover, four inversions have been identified in sub-sag B, the earliest of which took place until the terminal phase of the sedimentary period of Wenchang Formation. The earliest inversion was advantageous for the accumulation of oil and gas as the structural trap was formed earlier than the hydrocarbon expulsion period of the source rocks. As a result of uplifted inversion structure, the water is relatively shallower along the southern boundary fault, fostering the development of sand bodies. Since the source rocks for the middle-deep lacustrine facies of the Wenchang Formation lean upward in sub-sag B to the south, it can be interpreted that the downthrown side of the North Branch of the West Part of the Zhu III South Fault is a favorable area for oil and gas migration and accumulation near the boundary fault (Zhang et al., 2009). Hence, the deep stratigraphy of the sub-sag B in the inversion area is a profitable position for oil and gas exploration.

Strike-slip components may occur when the direction of regional stress in the later period intersects obliquely with the strike of pre-existing faults (Bott, 1959). It has been well studied that the degree of the strike-slip component largely depends on its strength and the scale of pre-existing faults. If the pre-existing fault is bent or staggered, the strike-slip component may have triggered restraining area and releasing area in its bending or staggered portions (Lowell, 1985; Harding, 1985). In particular, the numerous inversions of sub-sag B are typical illustration of the inversion structure created by the strike-slip component at the restraining bend of the boundary fault called Zhu III South Fault. Moreover, JX1-1 structure in Liaodongwan Depression of Bohai Bay Basin is an example of inversion structures formed in Liaozhong Fault (a part of Tanlu strike-slip fault zone) at its restraining bend (Qiang et al., 2012; Teng et al., 2017).

Three sub-sags in Wenchang Sag have developed differently, serving as a reminder in basin analysis that the effect of a shift in regional stress direction should not be disregarded. When the direction of regional stress deflects, the pre-existing fault can produce strike-slip component, forming restraining bends or releasing bends that the former bends form a reversion structure, or uplift and erosion, and the latter ones superimpose pull-apart subsidence. It is apparent that the conditions of oil and gas generation and accumulation between restraining bends and releasing bends are dissimilar, thus having an impact on our interpretation of the primary control factors of the reservoir and the adjustment of exploration ideas.

#### 6 Conclusions

- (1) Based on the statistics of the growth faults in 12 stratigraphic interfaces, we suggest that the direction of the regional tensile stress rotated clockwise from WNW-ESE in the Paleocene to NW-SE and NNW-SSE in the Eocene, to nearly S-N in the Oligocene and eventually to NNE-SSW in the Miocene
- (2) As the boundary fault in the southern margin of the Wenchang Sag, the Zhu III South Fault trends in NE in general and is arc-shaped in the plane. The direction of the regional tensile stress rotated clockwise and was not perpendicular to the existing fault, which resulted in a of strike-slip stress component. Therefore, the restraining bends and releasing bend were developed at the bent part of the fault, leading to compressional inversion and pull-apart subsidence in the different sub-sags. The strike-slip component of the Zhu III South Fault became stronger when the intersection angle between the regional tensile direction and the tensile stress decreased. As the intersection angle between the regional tensile stress direction and the strike of the Zhu III South Fault declined to some degree, the strike-slip component increased. As the regional tensile stress enlarged to some extent, the intensity of the strike-slip component also increased.
- (3) The different deformation characteristics and tectonic evolutions of the sub-sags in the Wenchang Sag in the PRMB are as follow: 1) The evolution of sub-sag B evolved four structural inversions. 2) Due to the intense compressional uplift and erosion during the depositional period of Enping Formation, subsidence in sub-sag C may have ceased. 3) In response to the superposition of the extension and the pullapart components, sub-sag An underwent continuous subsidence. The dynamic mechanism involved the formation of the restraining bend and the releasing bend on the arcuate Zhu III South Fault as a consequence of the differential local stress caused by clockwise rotation of the direction of the regional tensile stress. As a result of the regional tectonic movement, the change in the regional stress direction and the influence of the pre-existing curved faults, the adjacent sub-sags exhibit obvious differences in terms of their subsidence, sedimentation, oil and gas generation, and structural characteristics. This provide a novel concept for analyzing basin structures and guiding oil and gas exploration.

## **Declaration of competing interest**

The authors declare that they have no known competing financial interests or personal relationships that could have appeared to influence the work reported in this paper.

## Acknowledgements

This work was financially supported by the National Natural Science Foundation of China (Grant No. 91328201; 42006068) and Shandong Special Fund of Qingdao National Laboratory of Marine Science and Technology (No. 2021QNLM020001-1). We sincerely thank Hainan Branch of the China National Offshore Oil Corporation for providing data and support for this work. We are grateful to all reviewers for their thorough and constructive reviews, which greatly helped to improve our manuscript.

#### References

- Acocella, V., Gudmundsson, A., Funiciello, R., 2000. Interaction and linkage of extension fractures and normal faults: examples from the rift zone of Iceland. J. Struct. Geol. 22 (9), 1233–1246. https://doi.org/10.1016/S0191-8141(00) 00031-6
- Allen, A.P., Allen, R.J., 1990. Basin Analysis Principles and Applications. Blackwell publishing Ltd, 1–549.
- Anderson, E.M., 1951. The Dynamics of Faulting and Dyke Formation with Application to Britain. Oliver and Boyd, Edinburgh, pp. 1–206.
- Bao, X.H., Ji, Y.B., Hu, Y., et al., 2017. Geochemical characteristics, origins, and model of lacustrine source rocks in the Zhu 1 depression, eastern Pearl River Mouth Basin, South China Sea. AAPG (Am. Assoc. Pet. Geol.) Bull. 101 (9), 1543–1564. https://doi.org/10.1306/11071614117.
- Bott, M.H.P., 1959. The mechanics of oblique slip faulting. Geo. Mag. 96 (2), 109–117. https://doi.org/10.1017/S0016756800059987.
- Briais, A., Patriat, P., Tapponnier, P., 1993. Updated interpretation of magnetic anomalies and seafloor spreading stages in the south China sea implications for the tertiary tectonics of southeast Asia. J. Geophys. Res. Solid Earth (B4), 6299–6328. https://hal.archives-ouvertes.fr/hal-00552239.
- Cai, Z.R., Liu, W.L., Wan, Z.F., et al., 2010. Determination of Cenozoic tectonic movement in the northern South China Sea and the relationship between oilgas reservoir and tectonic movement. Mar. Sci. Bull. 29 (2), 161–165 (in Chinese).
- Cembrano, J., González, G., Arancibia, G., et al., 2005. Fault zone development and strain partitioning in an extensional strike-slip duplex: a case study from the Mesozoic Atacama fault system, Northern Chile. Tectonophysics 400, 105–125. https://doi.org/10.1016/j.tecto.2005.02.012.
- Cheng, P., Tian, H., Huang, B.J., et al., 2013. Tracing early-charged oils and exploration directions for the wenchang A sag, western Pearl River Mouth basin, offshore South China sea. Org. Geochem. 61 (6), 15–26. https://doi.org/10.1016/j.orggeochem.2013.06.003.
- Contreras, J., Anders, M.H., Scholz, C.H., 2000. Growth of a normal fault system: observations from the lake Malawi basin of the east african rift. J. Struct. Geol. 22 (2), 159–168. https://doi.org/10.1016/S0191-8141(99)00157-1.
- Cunningham, W.D., Mann, P., 2007. Tectonics of strike-slip restraining and releasing bends. Geol. Soc. Lond. Spec. Publ. 290, 1–12.
- Deng, G.J., Zhang, Y.Z., Gan, J., 2012. Pulsating tectonic evolution and its relationship with hydrocarbon accumulation in Wenchang B Depression. Fault-Block Oil Gas Field 19 (5), 564–567. https://doi.org/10.6056/dkyqt201205005 (in Chinese).
- Deng, H.D., Ren, J.Y., Pang, X., et al., 2020. South China sea documents the transition from wide continental rift to continental break up. Nat. Commun. 11 (1), 4583. https://doi.org/10.1038/s41467-020-18448-y.
- Dooley, T.P., Schreurs, G., 2012. Analogue modelling of intraplate strike-slip tectonics: a review and new experimental results. Tectonophysics 1–71. https://doi.org/10.1016/j.tecto.2012.05.030, 574–575.
- Gan, J., Zhang, Y.Z., Deng, Z.Y., et al., 2012. Reservoir-forming characteristic and model of the palaeogene condensate gas reservoir with low permeability in wenchang a sag. Nat. Gas Geosci. 23 (6), 1060–1069 (in Chinese).
- Gan, J., Xie, Y.H., Zhang, Y.Z., et al., 2014. A relationship between abnormally high pressure in Enping Formation and hydrocarbon accumulation in Wenchang A sag. China Offshore Oil Gas 23 (6), 7–13 (in Chinese).
- Ghosh, N., Chattopadhyay, A., 2008. The initiation and linkage of surface fractures above a buried strike-slip fault: an experimental approach. J. Earth Syst. Sci. 117 (1), 23–32. https://doi.org/10.1007/s12040-008-0009-y.
- Guo, L.Z., Zhong, Z.H., Wang, L.S., et al., 2001. Regional tectonic evolution around yinggehai basin of South China sea. Geol. J. China Univ. 7 (1), 1–12 (in Chinese).
- Hall, R., 2012. Late Jurassic-cenozoic reconstructions of the Indonesian region and the indian ocean. Tectonophysics 570–571 (11), 1–41. https://doi.org/10.1016/ j.tecto. 2012.04.021.
- Hall, R., van Hattum, M.W., Spakman, W., 2008. Impact of India—Asia collision on SE Asia: the record in borneo. Tectonophysics 451 (1–4), 366–389. https://doi.org/10.1016/j.tecto.2007.11.058.
- Harding, T.P., 1985. Seismic characteristics and identification of negative flower structures, positive flower structures, and positive structural inversion. AAPG Bull. 69 (4), 582–600. https://doi.org/10.1306/AD462538-16F7-11D7-8645000102C1865D.
- He, J.X., Chen, S.H., Ma, W.H., et al., 2012. The evolution, migration and accumulation regularity of oil and gas in Zhujiangkou basin, northeastern South China Sea. Chin. Geol. 39 (1), 106–118 (in Chinese).
- He, M., Zhong, G.F., Liu, X.F., et al., 2017. Rapid post-rift tectonic subsidence events in the Pearl River Mouth basin, northern South China Sea margin. J. Asian Earth Sci. 147, 271–283. https://doi.org/10.1016/j.jseaes.2017.07.024.

  Hsiao, L., Graham, S.A., Tilander, N., 2004. Seismic reflection imaging of a major
- Hsiao, L., Graham, S.A., Tilander, N., 2004. Seismic reflection imaging of a major strike-slip fault zone in a rift system: paleogene structure and evolution of the Tan-Lu fault system, Liaodong Bay, Bohai, offshore China. AAPG Bull. 88, 71–97. https://doi.org/10.1306/09090302019.
- Huang, B.J., Li, J.L., Li, L., et al., 2007. A discussion on the hydrocarbon accumulation characteristics and distribution in Wenchang A sag. China Offshore Oil Gas 19 (6), 361–366 (in Chinese).
- Huang, B.J., Xiao, X.M., Zhang, M.Q., 2003. Geochemistry, grouping and origins of crude oils in the western Pearl River Mouth basin, offshore South China sea. Org. Geochem. 34 (7), 993–1008. https://doi.org/10.1016/S0146-6380(03) 00035-4.

Hutchison, C.S., 2004. Marginal basin evolution: the southern south China sea. Mar. Petrol. Geol. 21 (9), 1129–1148. https://doi.org/10.1016/j.marpetgeo.2004.07.002.

- Ingram, G.M., Chisholm, T.J., Grant, C.J., et al., 2004. Deepwater north west borneo: hydrocarbon accumulation in an active fold and thrust belt. Mar. Petrol. Geol. 21 (7), 879–887. https://doi.org/10.1016/j.marpetgeo.2003.12.007.
- Jackson, E.D., Shaw, H.R., Bargar, K.E., 1975. Calculated geochronology and stress field orientations along the Hawaiian chain. Earth Planet Sci. Lett. 26 (2), 145–155. https://doi.org/10.1016/0012-821X(75)90082-5, 5.
- Jiang, H., Wang, H., Xiao, J., et al., 2008. Tectonic inversion and its relationship with hydrocarbon accumulation in zhu-3 depression of pearl river mouth basin. Acta Pet. Sin. 29 (3), 372–377 (in Chinese).
- Jiang, R.F., Zhou, J.X., Yang, X.B., et al., 2020. The different extension and strike-slip mechanism and its accumulation controlling effect in Wenchang B sag. Acta Geol. Sin. 94 (8), 2422–2432 (in Chinese).
- Lee, T.Y., Lawer, T.A., 1995. Cenozoic plate reconstruction of Southeast Asia. Tectonophysics 251 (1–4), 85–138. https://doi.org/10.1016/0040-1951(95)00023-2. Lei, B.H., Zheng, Q.G., Li, J.L., et al., 2012. Formation and evolution of Zhu-3 south
- Lei, B.H., Zheng, Q.G., Li, J.L., et al., 2012. Formation and evolution of Zhu-3 south fault and its control on the depocenter shift in Zhu-3 depression, Pearl River Mouth Basin. Shiyou Xuebao/Acta Petrolei Sinica 33 (5), 807—813 (in Chinese).
- Li, C., Zhang, Y.Z., You, L., et al., 2014. Accumulation conditions and potential analyses of Wenchang C sag in Pearl River Mouth basin. Petrol. Geol. Exper. 36 (3), 346–351 (in Chinese).
- Li, G., Mei, L.F., Pang, X., et al., 2022. Magmatism within the northern margin of the South China Sea during the post-rift stage: an overview, and new insights into the geodynamics. Earth Sci. Rev. 225, 103917. https://doi.org/10.1016/j.earscirev.2022.103917.
- Li, H., Zhang, Y.Z., Gan, J., et al., 2014. The style distribution and hydrocarbon accumulation of inverted structures in Zhu-3 depression, 2014 J. Oil Gas Technol. (J. Jianghan Petroleum Inst.) 36 (4), 1–6 (in Chinese).
- Li, H., Zhang, Y.Z., Niu, C.Y., et al., 2015. Hydrocarbon accumulation pattern of wenchang B sag, western Pearl River Mouth basin in the Northern South China sea. Mar. Geol. Quat. Geol. 35 (4), 133–139 (in Chinese).
- Li, P.L., 1993. Cenozoic tectonic movement in the pearl river mouth basin. China Offshore Oil Gas 7 (6), 11–17 (in Chinese).
- Liu, L.L., Zhang, J.L., Sun, Z.Q., et al., 2019. Constraints of three-dimensional geological modeling on reservoir connectivity: a case study of the huizhou depression, pearl river mouth basin, south China sea. J. Asian Earth Sci. 171, 144–161. https://doi.org/10.1016/j.jseaes.2018.09.014. MAR.
- Liu, Y., Xu, Z.M., Zhao, R.Q., et al., 2022. Trace rare earth elements in the Enping Formation of Wenchang A sag and its implications for paleoproduction environment. Arabian J. Geosci. 15 (7), 1–12. https://doi.org/10.1007/s12517-022-09842-5.
- Lowell, J.D., 1985. Structural styles in petroleum geology. OGCI, the United States of America.
- Lu, J., Zhou, G., Zheng, R.F., et al., 2016. Oil origin and accumulation characteristics in middle-deep strata of Wenchang A sag, Pearl River Mouth basin. China Offshore Oil Gas 28 (1), 20–28 (in Chinese).
- Madon, M., Ly, K.C., Wong, R., 2013. The structure and stratigraphy of deepwater Sarawak, Malaysia: implications for tectonic evolution. J. Asian Earth Sci. 76, 312–333. https://doi.org/10.1016/j.jseaes.2013.04.040.
- McClay, K.R., 1990. Extensional fault systems in sedimentary basins: a review of analogue model studies. Mar. Petrol. Geol. 7 (3), 206–233. https://doi.org/ 10.1016/0264-8172(90)90001-W.
- McClay, K., Bonora, M., 2001. Analog models of restraining step overs in strike-slip fault systems. AAPG (Am. Assoc. Pet. Geol.) Bull. 85, 233–260. https://doi.org/10.1306/8626C7AD-173B-11D7-8645000102C1865D.
- McClay, K.R., Ellis, P.G., 1987. Geometries of extensional fault systems developed in model experiments. Geology 15 (4), 341–344. https://doi.org/10.1130/0091-7613(1987)15<341:GOEFSD>2.0.CO;2.
- Miao, S.D., Xu, J.Y., Yin, B.H., et al., 2013. Inverted tectonic characters and prediction of potential area in zhu-3 depression of pearl river mouth basin. Nat. Gas Geosci. 24 (3), 566–573 (in Chinese).
- Mitra, S., Paul, D., 2011. Structural geometry and evolution of releasing and restraining bends Insights from laser-scanned experimental models. AAPG (Am. Assoc. Pet. Geol.) Bull. 95, 1147–1180. https://doi.org/10.1306/09271010060.
- Mu, D.L., Peng, G.R., Zhu, D.W., et al., 2022. Structure and formation mechanism of the Pearl River Mouth basin: insights from multi-phase strike-slip motions in the Yangjiang sag, SE China. J. Asian Earth Sci. 226, 1—17. https://doi.org/10.1016/j.jseaes.2022.105081.
- Naylor, M.A., Mandl, G., Sijpesteijn, C.H.K., 1986. Fault geometries in basement-induced wrench faulting under different initial stress states. J. Struct. Geol. 8, 737–752. https://doi.org/10.1016/0191-8141(86)90022-2.
- Northrup, C.J., Royden, L.H., Burchfiel, B.C., 1995. Motion of the Pacific plate relative to Eurasia and its potential relation to Cenozoic extension along the eastern margin of Eurasia. Geology 23 (8), 719–722. https://doi.org/10.1130/0091-7613(1995)023<0719: MOTPPR>2.3.CO;2.
- Pang, X., Chen, C.M., Zhu, M., et al., 2009. Baiyun movement: a significant tectonic event on Oligocene/miocene boundary in the northern south China sea and its regional implications. J. Earth Sci-China 20 (1), 49–56. https://doi.org/10.1007/ s12583-009-0005-4.
- Patton, T.L., 2005. Sandbox models of downward-steepening normal faults. AAPG Bull. 89 (6), 781–797. https://doi.org/10.1306/0105052001108.
- Peacock, D.C.P., 2002. Propagation, interaction and linkage in normal fault systems. Earth Sci. Rev. 58 (1–2), 121–142. https://doi.org/10.1016/S0012-8252(01)

00085-X

- Qiang, K.S., Lv, X.X., Zhou, X.H., et al., 2012. The inversion structure zone and reservoir history of the JX1-1 area in Liaodongwan depression, offshore Bohai Bay Basin. J. Mineral. Petrol. 32 (4), 31–40 (in Chinese).
- Quan, Y.B., Liu, J.Z., Hao, F., et al., 2018. Geochemical characteristics and origins of natural gas in the zhu iii sub-basin, pearl river mouth basin, China. Mar. Petrol. Geol. 101, 117–131. https://doi.org/10.1016/j.marpetgeo.2018.12.007.
- Quan, Y.B., Liu, J.Z., Zhao, F., et al., 2015. The origin and distribution of crude oil in Zhu III sub-basin, Pearl River Mouth Basin, China. Mar. Petrol. Geol. 66, 732–747. https://doi.org/10.1016/j.marpetgeo.2015.07.015.
- Rangin, C., Bellon, H., Benard, F., et al., 1990. Neogene arc-Continent collision in sabah, Northern borneo (Malaysia). Tectonophysics 183 (1–4), 305–319. https://doi.org/10.1016/0040-1951(90)90423-6.
- Ren, J.Y., Tamaki, K., Li, S.T., et al., 2002. Late mesozoic and cenozoic rifting and its dynamic setting in eastern China and adjacent areas. Tectonophysics 344 (3—4), 175—205. https://doi.org/10.1016/S0040-1951(01)00271-2, 2002.
- Robson, A.G., Holford, S.P., King, R.C., et al., 2018. Structural evolution of horst and half-graben structures proximal to a transtensional fault system determined using 3D seismic data from the Shipwreck Trough, offshore Otway Basin, Australia. Mar. Petrol. Geol. 89, 615–634. https://doi.org/10.1016/j.imarnetgeo.2017.10.028
- Ru, K., Pigott, J.D., 1986. Episodic rifting and subsidence in the South China sea. AAPG (Am. Assoc. Pet. Geol.) Bull. 70, 1136–1155. https://doi.org/10.1306/94886A8D-1704-11D7-8645000102C1865D
- Schlische, R.W., Withjack, M.O., Eisenstadt, G., 2002. An experimental study of the secondary deformation produced by oblique-slip normal faulting. AAPG (Am. Assoc. Pet. Geol.) Bull. 86, 885–906. https://doi.org/10.1306/61EEDBCA-173E-11D7-8645000102C1865D.
- Sun, W.D., Zhang, L.P., Liao, R.Q., et al., 2020. Plate convergence in the Indo-Pacific region. J. Oceanol. Limnol. 38 (4), 1008–1017. https://doi.org/10.1007/s00343-020-0146-v.
- Teng, C.Y., Hao, F., Zou, H.Y., et al., 2017. Development and evolution of the structure JX1-1 in Liaodong Bay depression and its significance in petroleum exploration. Shiyou Diqiu Wuli Kantan/Oil Geophys. Prospect. 52 (3), 599–611 (in Chinese).
- Tong, H.M., 2010. Fault formation and evolution model under uncoordinated extension in rift basin. Geol. Bull. China 29 (11), 1606–1613 (in Chinese).
- Vail, P.R., Posamentier, H.W., 1988. Principles of Sequence Stratigraphy, vol. 15. Elsevier Science Ltd, pp. 1–572.
- Van Hinsbergen, D.J.J., Steinberger, B., Doubrovine, P.V., et al., 2011. Acceleration and deceleration of India-Asia convergence since the Cretaceous: roles of mantle plumes and continental collision. J. Geophys. Res. Solid Earth 116 (B6). https:// doi.org/10.1029/2010JB008051.
- Woodcock, N.H., 2003. Transpressive duplex and flower structure: dent fault system, NW England. J. Struct. Geol. 25, 1981–1992. https://doi.org/10.1016/S0191-8141(03)00057-9.

- Woodcock, N.H., Fischer, M., 1986. Strike-slip duplexes. J. Struct. Geol. 8 (7), 725–735. https://doi.org/10.1016/0191-8141(86)90021-0.
- Wu, C.L., 1984. Nanhai (the South China sea) movement and development of basins in the South China sea. Bull. Mar. Sci. 3 (2), 47–53 (in Chinese).
- Xiao, X.M., Li, N.X., Gan, H.J., et al., 2009. Tracing of deeply-buried source rock: a case study of the WC9-2 petroleum pool in the Pearl River Mouth Basin, South China Sea. Mar. Petrol. Geol. 26 (8), 1365–1378. https://doi.org/10.1016/j.marpetgeo.2009.02.009.
- Xie, Z.Y., Sun, L.T., Pang, X., et al., 2017. Origin of the dongsha event in the South China sea. Mar. Geophys. Res. 38 (4), 357–371. https://doi.org/10.1007/s11001-017-9321-8.
- You, L., Xu, S.L., Li, C., et al., 2018. Diagenesis-porosity evolution and "sweet spot" distribution of low permeability reservoirs: a case study from oligocene zhuhai Formation in wenchang a sag, pear river mouth basin, northern south China sea. Petrol. Explor. Dev. 45 (2), 251–263. https://doi.org/10.1016/S1876-3804(18)30028-4.
- Zhang, J.L., Wu, Z.C., Shen, Z.Y., et al., 2020. Seismic evidence for the crustal deformation and kinematic evolution of the Nansha Block, South China Sea. J. Asian Earth Sci. 203, 104536.
- Zhang, Y.H., Gan, J., Deng, Y., et al., 2009. Hydrocarbon plays in Wenchang B sag and its surrounding areas, the western Pearl River Mouth basin. China Offshore Oil Gas 21 (5), 303–307 (in Chinese).
- Zhang, Y.Z., Chen, Z.H., Li, X.S., et al., 2011. Petroleum accumulation characteristics and favorable exploration directions in Wenchang B Sag and its surrounding areas, Pearl River Mouth Basin, 2011 Petrol. Geol. Exper. 33 (3), 297–302 (in Chinese).
- Zhang, Y.Z., Gan, J., Li, H., et al., 2013. Strike-slip deformation mechanism and its petroleum geology significance along south fault in Zhu III depression under extensional tectonic setting. China Offshore Oil Gas 25 (5), 9–15 (in Chinese).
- Zhao, S.J., Wu, S.G., Shi, H.S., et al., 2012. Structures and dynamic mechanism related to the dongsha movement at the northern margin of south China sea. Prog. Geophys. 27 (3), 1008–1019 (in Chinese).
- Zhong, Ž., Liu, F., Weijun, H.E., et al., 2018. Sedimentary facies in oligocene zhuhai member-2 in wenchang sag and adjacent area, Pearl River Mouth basin. Mar. Origin Petrol. Geol. 23 (3), 53–64 (in Chinese).
- Zhou, D., Ru, K., Chen, H.Z., 1995. Kinematics of cenozoic extension on the south China sea continental margin and its implications for the tectonic evolution of the region. Tectonophysics 251 (1–4), 161–177. https://doi.org/10.1016/0040-1951(95)00018-6.
- Zhu, H.T., Li, S., Shu, Y., et al., 2016. Applying seismic geomorphology to delineate switched sequence stratigraphic architecture in lacustrine rift basins: an example from the Pearl River Mouth Basin, northern South China Sea. Mar. Petrol. Geol. 78 (4), 785–796. https://doi.org/10.1016/j.marpetgeo.2015.12.013.
- Zhu, W.L., Mi, L.J., 2011. Atlas of Oil and Gas Basins, China Sea. Petroleum Industry Press, Beijing, pp. 106–107 (in Chinese).